Chiral superfluid phase of liquid ³He in planar aerogels

Tomohiro Hisamitsu and Ryusuke Ikeda

Department of Physics, Kyoto University, Kyoto 606-8502, Japan

Motivated by the realization of the chiral superfluid phase of liquid ³He stabilized at lower pressures and over a wide temperature range in planar aerogels, we examine equilibrium properties of the superfluid *A* phase suffering from impurity scatterings due to planar correlated defects. In the specular limit of scattering due to the planar defects, an analog of Anderson's theorem for the *s*-wave Fermi superfluid is well satisfied in the chiral *A* phase in the planar aerogels just like in the polar phase in nematic aerogels, and the chiral *A* phase region is extended by such a planar anisotropy even with no strong coupling correction. It is also pointed out that the vortex energy in the chiral *A* phase depends on the relative sense of the vorticity to the chirality. Based on this result, it is argued that, due to the presence of chiral domains induced by the randomness, the vortex lattice structure shows broken time-reversal symmetry and may include vortex loops.

I. INTRODUCTION

Recent NMR measurements in liquid ³He in strongly anisotropic aerogels have clarified that the degeneracy in energy between different pairing states can easily be lifted by quasiparticle scattering events due to the aerogel. In the nematic aerogels composed of columnar defects, the superfluid ³He was found to be in the one-dimensional (1D) polar pairing state over wide temperature and pressure ranges [1]. This observation is in qualitative agreement with the expectation [2] following from a weak stretched anisotropy, while a model starting from the limit of strong 1D-like anisotropy was necessary to explain the realization of the polar phase extending over a *broad* temperature and pressure range [3,4]. In the opposite case with a compressional anisotropy, a chiral superfluid phase, i.e., the *A* phase with a perpendicular orientation of its **l** vector to the easy plane for Cooper pairs, is expected [2] to be realized even at lower pressures where the so-called strong-coupling correction [5,6] is negligible.

Such a chiral *A* phase stabilized over lower pressures has been found recently in liquid ³He in several aerogel materials [7,8]. In recent experiments using planar aerogels [8] in which the strands are randomly oriented within a fixed plane, the chiral *A* phase with its **l** vector oriented perpendicularly to the plane is seen over wide pressure and temperature ranges. Among the planar aerogel samples [8], the liquid ³He in mullite aerogel shows a notable depression of the superfluid transition temperature $T_c(P)$ and a wide *A* phase region in the pressure (*P*)-temperature (*T*) phase diagram, indicating a strong impurity scattering effect and a large planar anisotropy. On the other hand, the nylon aerogel sample [8] with a similar *A* phase extending over broad temperature and pressure ranges has shown $T_c(P)$ in close vicinity of the superfluid transition temperature $T_{c0}(P)$ of the bulk liquid. This feature in the latter aerogel sample suggests that an analog of Anderson's theorem [3,4,9,10] is satisfied even for the *A* phase in the

planar case like for the polar phase in the nematic aerogels and implies that a model representing strong anisotropy of such a planar aerogel is necessary to describe the resulting chiral *A* phase realized in a wide region in the phase diagram.

In this work, equilibrium properties of the chiral *A* phase suffering from impurity scatterings due to planar correlated defects are studied. Putting much importance on the phase diagram in the case of the nylon planar aerogel in Ref. [8], we examine the weak-coupling *P*-*T* phase diagram following from scattering models covering the limit of strong two-dimensional (2D) anisotropy. The chiral *A* phase is stabilized over a wide temperature range at any pressure by strong anisotropy. Similarly to Anderson's theorem [9] for the *s*-wave Fermi superfluids, the transition temperature $T_c(P)$ between the *A* phase and the normal liquid in the situation with a moderately strong 2D anisotropy is highly insensitive to the strength of the impurity scattering just like the corresponding one in nematic aerogels [3,4]. Nevertheless, the low *T* behavior of the quasiparticle energy gap is deviated at relatively low temperatures from the T^4 behavior resulting from the pointlike gap nodes which, in clean limit, is satisfied even at higher temperatures than $0.5T_{c0}(P)$. This feature is in contrast to the robustness of the corresponding T^3 behavior in the polar phase [4]. Next, we focus our attention on the energy of a half-quantum vortex (HQV) line oriented perpendicularly to the planar defects of the aerogel which depends on the relative sense between the vorticity and the **l** direction, i.e., the chirality. By taking account of the fact that the **l** vector is pinned by the planar defects in the aerogels, we will discuss how such a dependence of the vortex energy on the chirality is reflected in the resulting vortex lattice structure in the rotating system.

The present paper is organized as follows. In Sec. II, a model for the impurity scattering due to the defects in the planar aerogel is introduced, and the resulting phase diagram and the energy gap are discussed. In Sec. III, the HQV and
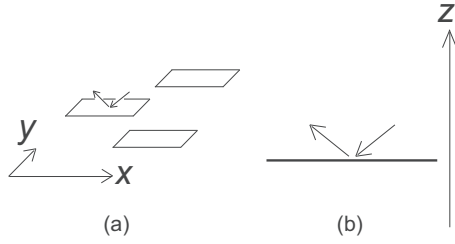
FIG. 1. Schematic pictures describing scattering events of normal quasiparticles via 2D-like (planar) defects lying in the x-y plane.

the conventional phase vortex (PV) are examined within the Ginzburg-Landau (GL) approach including the planar impurity scattering effect, and the expected vortex lattice including antivortices is discussed. In Sec. IV, the results in the present work are summarized.

II. ANALOG OF ANDERSON'S THEOREM FOR CHIRAL SUPERFLUID IN PLANAR AEROGELS

We start from describing the nonmagnetic scattering potential modeling the planar aerogels [8]. Throughout this paper, the 2D plane characterizing the structure of these aerogels will be identified hereafter as the x-y plane. By analogy to the columnar defects stabilizing the polar pairing state, we introduce a model of the impurity potential which can describe the scattering events in the *limit* of strong 2D anisotropy. In this limit, the x-y components of the quasiparticle momentum are not changed through an impurity scattering event, or equivalently, the correlation between the random scattering potential $u(\mathbf{r})$ is infinite-ranged along the x-y plane. Here, $u(\mathbf{r})$ is defined through the Hamiltonian describing the impurity scattering events

$$\mathcal{H}_{\mathrm{imp}} = \int d^3\mathbf{r}\, u(\mathbf{r})n(\mathbf{r}), \tag{1}$$

and $n(\mathbf{r})$ is the particle density operator. This term is added to the BCS Hamiltonian which will be given below.

We imagine that a planar aerogel is a collection of planar defects. Each of them has mesoscopic area, and its normal vector is along the z axis. Figure 1 is a rough picture on a quasiparticle scattering in such a planar aerogel. As an analytically tractable model of the correlator of the random potential $u(\mathbf{r})$, we adopt

$$W(\mathbf{r}) = 2\pi N(0)\tau \langle u(\mathbf{r})u(0)\rangle_{\mathrm{imp}} = \frac{k_F^2}{4\pi^2}\delta(z)\exp\left(-\frac{|\mathbf{r}_\perp|^2}{2L_\perp^2}\right), \tag{2}$$

where τ is the quasiparticle lifetime, $N(0)$ the density of states of the normal quasiparticle lying on the Fermi surface, k_F the Fermi wave number, $\mathbf{r}_\perp$ the projection onto the x-y plane of the coordinate $\mathbf{r}$, and $L_\perp$ is the correlation length defined along the x-y plane. Below, the Fourier transform of $W(\mathbf{r})$

$$w(\mathbf{p}-\mathbf{p}') = \frac{\delta_D}{2\pi}\exp\left(-\frac{1}{2}L_\perp^2(\mathbf{p}_\perp - \mathbf{p}'_\perp)^2\right) \tag{3}$$

will be used, where $\mathbf{p}_\perp$ is the projection onto the x-y plane of the momentum $\mathbf{p}$ on the Fermi surface, and $\delta_D = k_F^2 L_\perp^2$. In the limit of the strong planar anisotropy where $\delta_D \to \infty$, each

quasiparticle scattering is specular. We note that the model (3) cannot be used in $\delta_D \to 0$ limit which erroneously yields the clean limit. Hereafter, δ_D will be implicitly assumed to be nonvanishing.

The planar anisotropy favors 2D-like pairing states [2,11,12]. By choosing one of the 2D-like pairing symmetries (see below), the quasiparticle energy gap $|\Delta|$, which is also the amplitude of the p-wave order parameter field $A_{\mu,j}$, is determined through the total Hamiltonian $\mathcal{H} = \mathcal{H}_{\mathrm{BCS}} + \mathcal{H}_{\mathrm{imp}}$, where

$$\mathcal{H}_{\mathrm{BCS}} - \mu N = \sum_{\mathbf{p},\sigma}\left[\xi_\mathbf{p} a^\dagger_{\mathbf{p},\sigma}a_{\mathbf{p},\sigma} - \frac{1}{2}(\Delta_{\mathbf{p},\sigma}a^\dagger_{-\mathbf{p},\sigma}a^\dagger_{\mathbf{p},\sigma}\right.$$
$$\left. + \mathrm{H.c.})\right] + \frac{V}{3|g_{\mathrm{BCS}}|}A^*_{\mu,j}A_{\mu,j}, \tag{4}$$

g_{BCS} is the coupling constant measuring the attractive interaction, V is the system volume, and $\xi_\mathbf{p}$ is the quasiparticle energy measured from the Fermi energy μ. The gap function $\Delta_{\mathbf{p},\sigma}$ will be defined below.

As is well known, the Anderson-Brinkman-Morel (ABM) [5] and planar pairing states [13] belong to such candidates of the 2D-like pairing state. As far as the equilibrium thermodynamic properties are concerned, we can fix the direction of the gap node to the z axis. Then, the order parameter tensor of the ABM pairing, i.e., the chiral A phase, can be chosen to be $A_{\mu,j} = \Delta\hat{y}_\mu(\hat{y}-i\hat{x})_j$, while that of the planar pairing state is $A_{\mu,j} = \Delta(\delta_{\mu,j} - \hat{z}_\mu\hat{z}_j)$. Actually, in the present environment consisting of the planar defects, such a 2D-like pairing state is stabilized by directing the gap node along the z axis [14]. Alternatively, the 2×2 gap matrices of those states are diagonalized in the spin space, and their nonzero diagonal elements are

$$\Delta_{\mathbf{p},\sigma} = \Delta(\hat{p}_x + i\hat{p}_y) \equiv |\Delta_\mathbf{p}|e^{i\phi} \tag{5}$$

for the ABM state, and the corresponding one is

$$\Delta_{\mathbf{p},\sigma} = \Delta(\hat{p}_x + i\sigma\hat{p}_y) = |\Delta_\mathbf{p}|e^{i\sigma\phi} \tag{6}$$

for the planar pairing state, respectively, where $|\Delta_\mathbf{p}| = \Delta\sin\theta$, $\sigma = +1\,(-1)$ represents the spin-up (spin-down) state [11]. The momentum $\mathbf{p}$ is represented by the polar θ and the azimuthal ϕ angles, and θ is measured from the $+\hat{z}$ axis. We note that, in $\mathcal{H}_{\mathrm{BCS}}$, any spatial variation of Δ has been neglected here.

In our calculation in the present work, the strong-coupling correction stabilizing the bulk ABM state will be neglected to clarify that the 2D-like pairing states are stabilized only by a planar anisotropy. Then, as far as the spatiotemporal variations of the order parameter are neglected, each term of the GL expansion of the weak-coupling free energy functional is proportional to $\sum_{\mathbf{p},\sigma=\pm1}f(|\Delta_{\mathbf{p},\sigma}|^2)$ which takes the same value for the two pairing states. Further, each σ component contributes separately to the thermodynamic quantities. Therefore, in the present weak-coupling approach, the resulting thermodynamic properties are the same between the two pairing states [11]. We need not distinguish the ABM state from the planar one until considering the transition from the planar phase to the planar-distorted B phase, which is more 3D-like, at a lower temperature.

We can use almost the same formalism based on the Matsubara Green's functions as in the case of the s-wave superconductor [15] to describe thermodynamics of a spatially uniform planar pairing state in an impure environment. For the moment, our analysis will be preceded by assuming the 2D-like pairing state to be the planar one. Following the standard procedure [15] and the notation in the case of the polar phase in the columnar defects [4], the impurity-averaged diagonal $\mathcal{G}_{\mathbf{p}}(\varepsilon)$ and the off-diagonal $\mathcal{F}_{\mathbf{p},\sigma}(\varepsilon)$ Green's functions are represented in the form

$$
\overline{G}_{\mathbf{p},\sigma}(\varepsilon) = \begin{pmatrix} \mathcal{G}_{\mathbf{p}}(\varepsilon) & \mathcal{F}_{\mathbf{p},\sigma}(\varepsilon) \\ \mathcal{F}_{\mathbf{p},\sigma}^{\dagger}(\varepsilon) & -\mathcal{G}_{-\mathbf{p}}(-\varepsilon) \end{pmatrix}
$$
$$
= \frac{1}{\tilde{\varepsilon}_{\mathbf{p}}^2 + \xi_{\mathbf{p}}^2 + |\tilde{\Delta}_{\mathbf{p}}(\varepsilon)|^2} \begin{pmatrix} -i\tilde{\varepsilon}_{\mathbf{p}} - \xi_{\mathbf{p}} & -\tilde{\Delta}_{\mathbf{p},\sigma}(\varepsilon) \\ -[\tilde{\Delta}_{\mathbf{p},\sigma}(\varepsilon)]^* & -i\tilde{\varepsilon}_{\mathbf{p}} + \xi_{\mathbf{p}} \end{pmatrix}.
$$
(7)

Here, ε is a fermion Matsubara frequency, and

$$
i\tilde{\varepsilon}_{\mathbf{p}} = i\varepsilon - \overline{\mathcal{G}_{\mathbf{p}}(\varepsilon)}, \tag{8}
$$

$$
\tilde{\Delta}_{\mathbf{p},\sigma}(\varepsilon) \equiv |\tilde{\Delta}_{\mathbf{p}}(\varepsilon)|e^{i\sigma\phi} = \Delta_{\mathbf{p},\sigma} - \overline{\mathcal{F}_{\mathbf{p},\sigma}(\varepsilon)}. \tag{9}
$$

Self-consistently, the self-energy terms satisfy the relations

$$
\overline{\mathcal{G}_{\mathbf{p}}(\varepsilon)} \equiv g(\theta;\varepsilon) = \frac{1}{2\pi N(0)\tau} \int_{\mathbf{q}} w(\mathbf{p}-\mathbf{q})\,\mathcal{G}_{\mathbf{q}}(\varepsilon),
$$

$$
\overline{\mathcal{F}_{\mathbf{p},\sigma}(\varepsilon)} \equiv f(\theta;\varepsilon)e^{i\sigma\phi} = \frac{1}{2\pi N(0)\tau} \int_{\mathbf{q}} w(\mathbf{p}-\mathbf{q})[\mathcal{F}_{\mathbf{q},\sigma}^{\dagger}(\varepsilon)]^*,
$$
(10)

and the gap function $\Delta_{\mathbf{p},\sigma}$ yields the gap equation

$$
\Delta_{\mathbf{p},\sigma} = -|g_{\mathrm{BCS}}|T \sum_{\varepsilon} \int_{\mathbf{p}'} 3\frac{\mathbf{p}\cdot\mathbf{p}'}{p_{\mathrm{F}}^2} \mathcal{F}_{\mathbf{p}',\sigma}(\varepsilon). \tag{11}
$$

In the limit of infinite δ_D, we have

$$
w(\mathbf{p}-\mathbf{p}') \to k_{\mathrm{F}}^2 \delta^{(2)}(\mathbf{p}_\perp - \mathbf{p}'_\perp), \tag{12}
$$

and the resulting self-energy terms are given by $\overline{\mathcal{G}_{\mathbf{p}}(\varepsilon)}/(i\varepsilon) = \overline{\mathcal{F}_{\mathbf{p},\sigma}(\varepsilon)}/\Delta_{\mathbf{p},\sigma} \to -1/(2\tau\sqrt{\varepsilon^2 + |\Delta_{\mathbf{p},\sigma}|^2})$. Then, just like Anderson's theorem [9,15] for the s-wave superconductors, the gap equation reduces to the τ-independent expression for the bulk liquid.

For finite δ_D values, the quantities $g(\theta;\varepsilon)$ and $f(\theta;\varepsilon)$ satisfy the relations

$$
g(\theta;\varepsilon) = \frac{\delta_D}{4\pi\tau} \int_0^{\pi/2} d\theta' \sin\theta' \exp\left(-\frac{\delta_D}{2}(\sin^2\theta + \sin^2\theta')\right) I_0(\delta_D \sin\theta \sin\theta') \frac{-i\varepsilon + g(\theta',\varepsilon)}{\sqrt{[\varepsilon + ig(\theta',\varepsilon)]^2 + |\Delta\sin\theta' - f(\theta',\varepsilon)|^2}},
$$

$$
f(\theta;\varepsilon) = \frac{\delta_D}{4\pi\tau} \int_0^{\pi/2} d\theta' \sin\theta' \exp\left(-\frac{\delta_D}{2}(\sin^2\theta + \sin^2\theta')\right) I_1(\delta_D \sin\theta \sin\theta') \frac{-\Delta\sin\theta' + f(\theta',\varepsilon)}{\sqrt{[\varepsilon + ig(\theta',\varepsilon)]^2 + |\Delta\sin\theta' - f(\theta',\varepsilon)|^2}}, \tag{13}
$$

where $I_n(x) = (2\pi)^{-1}\int_0^{2\pi} \cos(n\phi)\exp(x\cos\phi)d\phi$ is the modified Bessel function of the first kind of order n. By representing the pressure-dependent coupling constant g_{BCS} in terms of the superfluid transition temperature $T_{c0}(P)$ of the bulk liquid, the corresponding gap equation takes the form

$$
\Delta \ln\left(\frac{T}{T_{c0}(P)}\right) = \pi T \sum_{\varepsilon} \left[\frac{3}{2}\int_0^{\pi/2} d\theta \sin^2\theta\left(\frac{\Delta\sin\theta - f(\theta;\varepsilon)}{\sqrt{[\varepsilon + ig(\theta;\varepsilon)]^2 + |\Delta\sin\theta - f(\theta;\varepsilon)|^2}}\right) - \frac{\Delta}{|\varepsilon|}\right]. \tag{14}
$$

The superfluid transition temperature T_c and the temperature dependence of the energy gap Δ of the planar phase in zero field are described in terms of Eqs. (13) and (14). Reflecting the fact that the low temperature superfluid phase of the bulk liquid is the B phase, i.e., the Balian-Werthamer (BW) pairing state [16], the high temperature 2D-like superfluid state in the planar aerogel tends to give way to the planar-distorted or 2D-like B phase at lower temperatures. This 2D-like B phase has the order parameter [2] $A_{\mu,j} = \Delta(\delta_{\mu,j} - \hat{z}_\mu\hat{z}_j) + \Delta_z\hat{z}_\mu\hat{z}_j$ with $|\Delta_z| \ll |\Delta|$ at least close to the continuous transition from the planar phase [2,11]. The position of this continuous transition between the two superfluid phases is determined, as performed elsewhere [4], by focusing on the Gaussian term of $O(\Delta_z^2)$ and is given by

$$
1 = |g_{\mathrm{BCS}}|T \sum_{\varepsilon} \int_{\mathbf{p}} \frac{p_z^2}{p_{\mathrm{F}}^2}[\mathcal{G}_{\mathbf{p},\sigma}(\varepsilon)\mathcal{G}_{-\mathbf{p},-\sigma}(-\varepsilon) - \mathcal{F}_{\mathbf{p},\sigma}^{\dagger}(\varepsilon)\mathcal{F}_{-\mathbf{p},-\sigma}^{\dagger}(-\varepsilon)], \tag{15}
$$

where the fact that the vertex p_z accompanying Δ_z is not dressed with the correlator (3) was used, and Δ_z was assumed to be real as well as Δ so that a higher planar to B transition temperature is obtained. More explicitly, the planar to B transition line is determined by

$$
\ln\left(\frac{T}{T_{c0}(P)}\right) = \pi T \sum_{\varepsilon} \left[\int_0^{\pi/2} d\theta \sin\theta \frac{3\cos^2\theta}{\sqrt{[\varepsilon + ig(\theta;\varepsilon)]^2 + |\Delta\sin\theta - f(\theta;\varepsilon)|^2}} - \frac{1}{|\varepsilon|}\right]. \tag{16}
$$

Of course, in real systems with a strong-coupling correction, the free energy of the chiral A phase is lowered compared with that of the planar phase, and the 2D-like phase to be realized at higher temperatures is the chiral A phase. This suggests that the A-B transition line may be lowered compared with the corresponding planar to B transition point in Fig. 2 (see below). On the other hand, the A-B transition is inevitably a discontinuous one, and its position seems to lie at
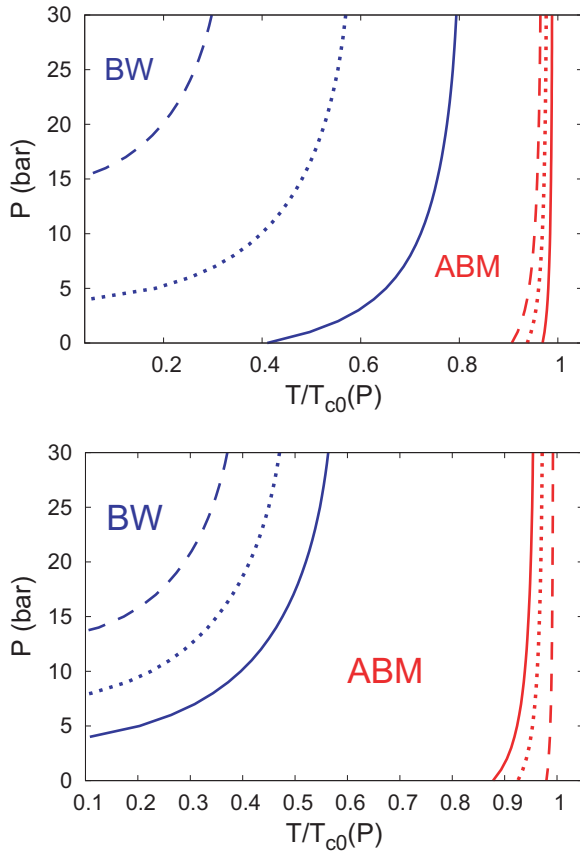
FIG. 2. Examples of the resulting pressure (P) to temperature (T) phase diagrams. Each *red* curve denotes the superfluid transition curve in each case. As noted in the text, the planar (high T) pairing state can be identified with the chiral or ABM pairing state, and each planar to B second order transition line (*blue* curve) is regarded as a reasonable estimate of the first order A-B transition curve in each case. In the upper figure, the two transition curves at a fixed anisotropy ($\delta_D = 10$) are described by increasing the scattering strength in the way $(2\pi\tau)^{-1}$(mK) = 0.5 (solid curves), 1.0 (dotted ones), and 1.5 (dashed ones), while, in the lower figure, they are described at a fixed impurity strength $(2\pi\tau)^{-1} = 1.2$ (mK) by increasing the anisotropy in the way $\delta_D = 5$ (solid curves), 10 (dotted ones), and 50 (dashed ones), respectively.

a higher temperature than the fictitious continuous transition point. Here, we primarily focus on the low pressure region in which the effects of the strong-coupling correction we have neglected here are weak enough, and hence, the deviation of the A-B transition point in equilibrium from the continuous transition point examined here should be sufficiently small. Further, depending on the cooling or warming rate in measurements, the A-B transition obtained experimentally or numerically will be accompanied by a notable hysteresis. Discussion about phenomena dependent on the experimental conditions is beyond the scope of the present work, and we will identify the planar to B transition line obtained here with the real chiral A to planar-distorted B transition line which should be found under a sufficiently low cooling or warming rate.

Now, the pressure to temperature phase diagram consisting of the A and B superfluid phases and the normal phase will be

discussed. In Fig. 2, typical examples of the resulting phase diagram are presented which follow from Eqs. (13), (14), and (16) in terms of the pressure dependence [13] of the bulk superfluid transition temperature $T_{c0}(P)$. The overall behaviors of the dependences of the transition curves on the impurity strength $(T_{c0}\tau)^{-1}$ and the anisotropy δ_D are quite similar to the corresponding ones in the situation in a nematic aerogel [4]: As τ decreases, or equivalently, the porosity of the aerogel is reduced, both of the transition curves decrease. When, as noted in relation to Eq. (12), the 2D-like correlation of the random potential is fitted to the planar momentum dependence of the pairing function, the situation becomes similar to that of the s-wave Fermi superfluid for which the so-called Anderson's theorem is satisfied. That is, when the anisotropy is large enough, the superfluid transition temperature $T_c(P)$ can stay close to the $T_{c0}(P)$ curve of the bulk liquid even if the planar-distorted B phase is lost due to a small enough τ. Thus, a situation in which the only realized superfluid phase is the ABM pairing state easily occurs [7]. As mentioned in Sec. I, the superfluid phase diagram realized in the nylon sample [8] has shown a $T_c(P)$ line lying quite close to the $T_{c0}(P)$ line together with the A phase extending over a wide temperature range. These features seen in the experiment [8] are consistent with those in Fig. 2, suggesting that the experimental situation is close to the case in which the impurity scattering is nearly specular in the sense indicated in Fig. 1.

It will be valuable to compare the present superfluid ^{3}He in a planar aerogel with the corresponding system in a narrow slab [11,12]. Broadly speaking, the scattering time τ in the former corresponds to the film thickness in the latter. Further, as noted in Eq. (12), the limit of the strong 2D-like anisotropy in the former is nothing but the limit of the 2D specular scattering which is identical with the corresponding limit of the surface scattering in the latter. In fact, the superfluid transition temperature T_c in a narrow slab in the limit of the specular reflection is independent of the thickness [12]. However, in general, one cannot identify the mean-field phase diagram of a 3D system in a correlated random medium with that of a low dimensional system in a regular restricted geometry. For instance, in the case of thin slabs, the diffusive nature of the surface scattering is reflected in T_c through spatial variations of the order parameter [12], while the mean field T_c in the present 3D system is believed to be properly determined even with no gradient terms [17]. Further, the τ and T dependencies of the A-B phase boundary presented in Fig. 2 show no reentrant behavior of the type seen in a narrower slab [11].

In the 2D-like p-wave pairing state, the analog of Anderson's theorem for the conventional s-wave paired case may be seen not only in the phase diagram but also in the temperature dependence of the energy gap Δ. In Ref. [4], it has been pointed out that the T^3 behavior of $|\Delta(T)|$ in the polar pairing state originating from its line node is robust in a wide temperature region and visible until $0.6T_c$ even in a relatively dirty system where the polar-distorted A phase has already been lost at finite temperatures due to the impurity scatterings. For comparison, the corresponding power law of $|\Delta(T)|$ in the chiral phase in the planar aerogels will be considered. As usual, by focusing on the region close to the gap nodes on the Fermi surface, the low T behavior of the quasiparticle gap in
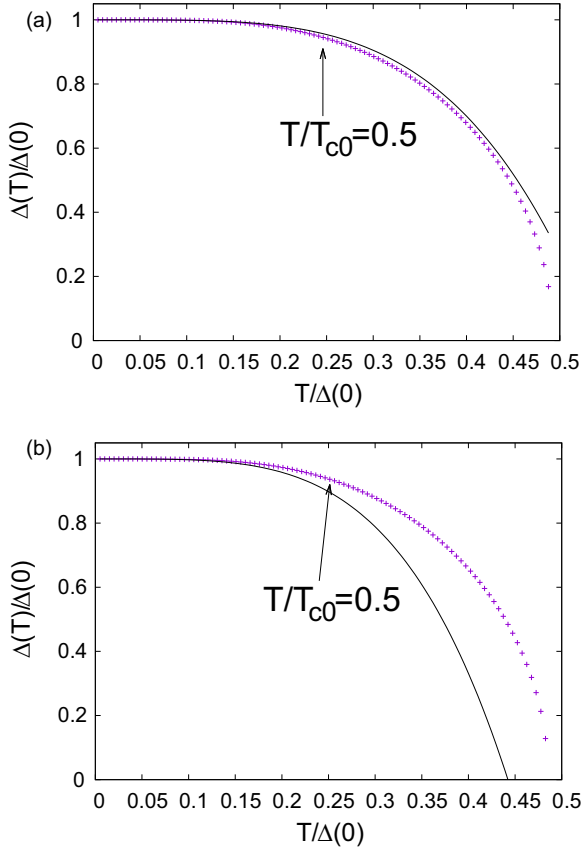
FIG. 3. Temperature dependence of the quasiparticle energy gap $|\Delta|$. Numerical data points are described in the case of the clean limit in the upper figure and, in the lower figure, in the present impure case with $(2\pi\tau)^{-1} = 2.0$ (mK) and $\delta_D = 50$ for which the B phase is absent even in $T \to 0$ limit. In both of the figures, the parameter values [13] at $P = 0$ (bar) have been used. Each solid curve denotes the best-fitted T^4 curve with $a_\perp = 11.73$ in (a) and the corresponding curve with $a_\perp = 26.12$ in (b), while the $\Delta(0)/T_{c0}$ value is 2.026 in (a) and 1.98 in (b). It is found that the ideal T^4 behavior is satisfied in the impure case only below $0.35T_c$. As noted in the text, this impurity scattering effect in the present planar aerogel seems to be remarkably different from the corresponding one in the nematic aerogel where the corresponding T^3 behavior is well satisfied over a wide temperature range even in the impure case [4].

the bulk A phase is found to obey

$$\Delta(T) \simeq \Delta(0)\left[1 - \tilde{a}_\perp\left(\frac{T}{\Delta(0)}\right)^4\right] \quad (17)$$

with $\tilde{a}_\perp = 7\pi^4/60 = 11.36$. The data points in Fig. 3(a) (the upper figure) are the corresponding results in the A phase in clean limit obtained by neglecting the strong-coupling correction. Note that the deviation from the T^4 behavior of Eq. (17) is relatively small even at higher temperatures. On the other hand, the corresponding behavior of Fig. 3(b) in the impure case indicates that the deviation from the T^4 behavior at higher temperatures is more remarkable, although the pointlike gap node is robust against the impurity scattering effect. We stress that this result has been obtained in the weak-coupling limit and, actually, at $P = 0$ (bar). It is possible that this deviation from the T^4 behavior in the impure case

becomes less remarkable by incorporating the strong-coupling correction.

III. VORTICES IN CHIRAL SUPERFLUID IN PLANAR AEROGELS

Now, we turn to examining possible vortex states in the chiral superfluid phase in the planar aerogel under a rotation around the z axis. Hereafter, we assume that the 2D-like pairing state is the ABM or chiral pairing state stabilized due to a weak but nonzero strong-coupling correction. Further, we will assume that no vortices are induced according to the Kibble-Zurek mechanism [18,19] by a supercooling in the present case because such a vortex occurring with no rotation should lie along the planar defects so that they are strongly pinned by the aerogel [20]. We primarily focus on the vortex lines induced by a rotation around the z axis, i.e., the vortices extending along the z axis perpendicular to the defect planes and hence, avoiding the strong pinning via the planar defects.

In the present situation where the **l** vector of the chiral phase is kept perpendicular to the defect plane, the stability of a pair of two HQVs [21] against the ordinary PV unaccompanied by a texture of the d vector can be considered. Far below the superfluid transition temperature, effects of the strong-coupling correction [21] and the dipole energy [22] destabilizing the HQVs are negligible and need not be considered hereafter. In such a dipole-free case, a texture of the d vector accompanying the HQV pair may be formed in any plane. Nevertheless, to be specific, the d vector will be assumed to lie in the x-y plane.

Conventionally, the order parameter structure far from the vortex core of a HQV in this situation has been studied in the London limit where no other order parameter components than that of the ABM pairing are excited, and the amplitude $|\Delta|$ of the ABM order parameter is fixed to be a constant. Then, when the sense (or, sign) of the phase winding number, i.e., of the vorticity, is the same as that of the orbital chirality, the ABM order parameter with one pair of HQVs is given by [23]

$$A_{\mu,j}^{(+)} = \Delta e^{i\Phi}(\hat{x}_\mu\cos\theta + \hat{y}_\mu\sin\theta)(\hat{e}_+)_j, \quad (18)$$

where

$$(\hat{e}_\pm)_j = \frac{\hat{x}_j \pm i\hat{y}_j}{\sqrt{2}}, \quad \Phi = \frac{1}{2}(\phi_+ + \phi_-), \quad \theta = \frac{1}{2}(\phi_+ - \phi_-), \quad (19)$$

and

$$\phi_\pm = \tan^{-1}\left(\frac{y}{x \mp a}\right). \quad (20)$$

As is well known, Eq. (18) can be rewritten in terms of the *spin* chirality basis

$$A_{\mu,j}^{(+)} = \frac{\Delta}{\sqrt{2}}[(\hat{e}_-)_\mu e^{i\phi_+} + (\hat{e}_+)_\mu e^{i\phi_-}](\hat{e}_+)_j. \quad (21)$$

On the other hand, the corresponding order parameter in the case where the sense of the vorticity is opposite to that of the (orbital) chirality

$$A_{\mu,j}^{(-)} \equiv A_{\mu,j}^{(+)}[(\hat{e}_+)_j \to (\hat{e}_-)_j] \quad (22)$$

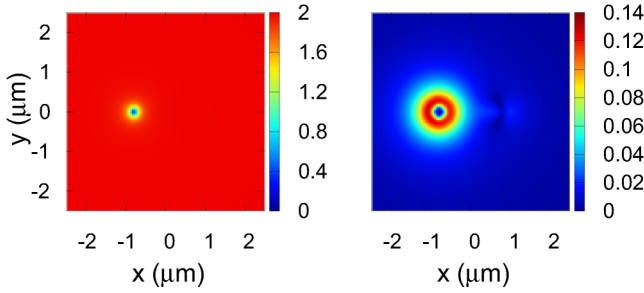is given by the complex conjugate of $A_{\mu,j}^{(+)}(\Phi \to -\Phi)$.

FIG. 4. Spatial distribution of the order parameter components accompanying a HQV lying at $(-a, 0)$ in the compatible case (see the text) at $P = 3$(bars) and $T = 1.0$(mK). This HQV and another one lying at $(a,0)$ forms one HQV pair with the size $2a = 1.6$ (μm). We note that $T_c[P = 3(\text{bar})] = 1.25$ (mK) for the parameter values $(2\pi\tau)^{-1} = 0.118$ (mK) and $\delta = 4.4$ characterizing the model aerogel used here [see Eq. (25)]. The left and right figures express $|A_{++}^{(+)}|$ and $|A_{+-}^{(+)}|$, respectively.

Alternatively, the order parameter $A_{\mu,j}^{(\pm)}$ may be represented in the form $\sum_{a,b=\pm} (\hat{e}_a)_\mu A_{ab}^{(\pm)} (\hat{e}_b)_j$. Then, Eq. (21) can be represented as $A_{-+}^{(+)} = \Delta e^{i\phi_+}/\sqrt{2}$, $A_{++}^{(+)} = \Delta e^{i\phi_-}/\sqrt{2}$, and, otherwise, zero. In the same manner, Eq. (22) is represented by $A_{--}^{(-)} = \Delta e^{i\phi_+}/\sqrt{2}$, $A_{+-}^{(-)} = \Delta e^{i\phi_-}/\sqrt{2}$, and, otherwise, zero. In the London limit with no dipole energy, the gradient energy is quadratic with respect to Φ [23] so that the sign change of Φ at a fixed orbital chirality does not lead to any change of the vortex energy. Thus, the broken time-reversal symmetry in the chiral A phase cannot be seen in thermodynamic properties associated with the vortices in the London limit.

Once going beyond the description in the London limit, however, a HQV in the ABM pairing state does not seem to be so simple: Each HQV derived numerically based on the GL free energy is accompanied close to its core by the order parameter component with a different orbital chirality. One example of a HQV derived in the present numerical work based on the GL model and the boundary condition (20) is presented in Fig. 4, where the **l** vector is directed to the $+z$ direction ($\hat{l} \parallel z$), and the winding number of this HQV is $+1/2$. According to Eq. (21), the left figure in Fig. 4 shows the spatial variation of $|A_{++}^{(+)}|$, while the right figure shows that of $|A_{+-}^{(+)}|$ which vanishes everywhere in the London limit. Essentially the same result has been presented in Refs. [21,24]. That is, it is found that a single HQV (a HQV pair) is described by *two* (*four*) of the nine complex scalar components of the order parameter $A_{\mu,j}$. Such an appearance of the component with the reversed orbital chirality suggests a possibility that the vortex energy depends on the relative sense between the vorticity and the orbital chirality. Previously, an effect of this relative sense on the observable quantity has been considered in the context of a chiral p-wave superconductivity [25].

In the present case with a uniaxial anisotropy, the resulting GL free energy density has the same form as used in Ref. [26] and consists of the condensation energy f_{cond} and the $O(|\Delta|^2)$ and $O(|\Delta|^4)$ gradient energy terms. Among them, f_{cond} takes

the form

$$
\begin{aligned}
f_{\text{cond}} = {}& [\alpha + (\alpha_z - \alpha)\delta_{iz}]A_{\mu i}A_{\mu i}^* + \beta_1 |A_{\mu i}A_{\mu i}|^2 \\
& + \beta_2 (A_{\mu i}A_{\mu i}^*)^2 + \beta_3 A_{\mu i}^* A_{\nu i}^* A_{\mu j}A_{\nu j} + \beta_4 A_{\mu i}^* A_{\nu i}A_{\nu j}^* A_{\mu j} \\
& + \beta_5 A_{\mu i}^* A_{\nu i}A_{\nu j}A_{\mu j}^* + \beta_z |A_{\mu z}A_{\mu z}^*|^2 \\
& + [\beta_{1z}A_{\mu i}A_{\mu i}A_{\mu z}^* A_{\mu z}^* + \beta_{2z}A_{\mu i}A_{\mu i}^* A_{\mu z}A_{\mu z}^* \\
& + \beta_{3z}A_{\mu i}^* A_{\nu i}^* A_{\mu z}A_{\nu z} + \beta_{4z}A_{\mu i}^* A_{\nu i}A_{\nu z}^* A_{\mu z} \\
& + \beta_{5z}A_{\mu i}^* A_{\nu i}A_{\nu z}A_{\mu z}^* + \text{c.c.}],
\end{aligned}
\tag{23}
$$

and the $O(|\Delta|^2)$ gradient energy terms of our interest are expressed by

$$
f_{\text{grad}}^{(2)} = 2K_1 \partial_i A_{\mu i}\partial_j A_{\mu j}^* + K_2 \partial_i A_{\mu j}\partial_i A_{\mu j}^* + K_4 \partial_i A_{\mu z}\partial_i A_{\mu z}^*.
\tag{24}
$$

In Eq. (24), z-derivative terms were neglected because we are interested here in the stability of the vortex lines extended along the z axis, i.e., perpendicular to the x-y plane or the defects' plane.

To make analytic evaluation of the coefficients appearing in f_{cond} and $f_{\text{grad}}^{(2)}$ easier, the simpler model

$$
w^{(\perp)}(\mathbf{k}) = \frac{\sqrt{\delta}}{1 + \delta \hat{k}_\perp^2}
\tag{25}
$$

for the correlator of the impurity potential was used in place of Eq. (3) in this section. In Eq. (25), $(\hat{\mathbf{k}}_\perp)_i = (\delta_{ij} - \hat{z}_i\hat{z}_j)k_j/k_F$, and δ is the parameter corresponding to δ_D in Eq. (3). This model is useful at least for moderate values of the anisotropy.

Derivation of the GL coefficients is essentially the same as in Ref. [26]. For instance, the coefficients of the quadratic mass terms are given by

$$
\alpha = \frac{1}{3}N(0)\left[\ln\left(\frac{T}{T_{c0}}\right) + 2\pi T \sum_{\varepsilon > 0}\left(\frac{1}{|\varepsilon|} - \frac{3}{2}I_{11}^{(\perp)}C_0^{(\perp)}\right)\right],
$$

$$
\alpha_z = \alpha - 2\pi T N(0) \sum_{\varepsilon > 0}\left[I_{10}^{(\perp)} - I_{11}^{(\perp)}\left(1 + \frac{1}{2}C_0^{(\perp)}\right)\right], \tag{26}
$$

where

$$
I_{mn}^{(\perp)} = \left\langle \frac{\hat{p}_\perp^{2n}}{|\tilde{\varepsilon}_p|^m}\right\rangle_{\hat{p}},
\tag{27}
$$

$$
\tilde{\varepsilon}_p = \varepsilon + \frac{\text{sgn}(\varepsilon)}{2\tau}\langle w^{(\perp)}(\mathbf{p} - \mathbf{p}_1)\rangle_{\hat{p}_1},
\tag{28}
$$

and $\langle\cdot\rangle_{\hat{p}}$ denotes the average over the direction of the unit vector $\hat{\mathbf{p}}$. Based on the notation in Eq. (4), the relation $i\tilde{\varepsilon}_p = \xi_{\mathbf{p}}$ gives, after the analytic continuation, the dispersion relation of a single quasiparticle in the normal fluid obtained within the Born approximation. Further,

$$
C_0^{(\perp)}(\varepsilon) = \frac{1}{1 - 2(I_{d11}^{(\perp)} - I_{d12}^{(\perp)})}
\tag{29}
$$

with

$$
I_{dmn}^{(\perp)}(\varepsilon) = \left\langle \frac{\sqrt{\delta}}{(2|\tilde{\varepsilon}_p|)^m \tau \left(1 + \delta \hat{p}_\perp^2\right)^n}\right\rangle_{\hat{p}}
\tag{30}
$$

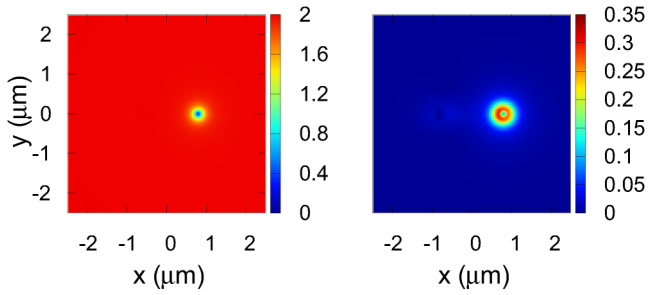is the ε-dependent factor representing the pairing vertex correction.

FIG. 5. Spatial distribution of the order parameter components accompanying a HQV existing at $(a, 0)$ in the incompatible situation. The winding number of this HQV is $+1/2$ as well as in Fig. 4. The parameter values used to obtain this solution are the same as those in Fig. 4. The left and right figures express $|A^{(-)}_{--}|$ and $|A^{(-)}_{-+}|$, respectively.

In addition to f_{cond} and $f^{(2)}_{grad}$, we need to incorporate the $O(|\Delta|^4)$ gradient energy terms to reach the correct understanding on the stability of HQVs within the GL analysis [21]. This higher order gradient energy inevitably becoming a lengthy expression has been presented in the Appendix of Ref. [21] as $f_{FLgrad4}$. In Ref. [26], the anisotropy-induced corrections to $f_{FLgrad4}$ arising from the impurity scattering process were examined, and it was found that they are safely negligible even in the limit of strong anisotropy. Hence, we have used $f_{FLgrad4}$ given in Ref. [21] using the typical value of the Landau parameter $F^{(s)}_1$ [13].

The numerical method we have used is the same as in the previous works [21,26]. The configuration of a HQV pair in the London limit was used as an initial condition of each numerical run. This initial configuration in the London limit plays the role of the outer boundary condition on the order parameter in the rectangle system. Throughout the present analysis, we have used the system of the size 40 (μm) in the x direction and the size 8 (μm) in the y direction.

It is found that all of the order parameter components such as $A_{\mu,z}$ vanish in the resulting vortex line solutions extending along the z axis in the chiral A phase of our interest, so that the terms of f_{cond} and $f^{(2)}_{grad}$ accompanied by the coefficients β_{nz}, β_z, and K_4 may not be taken into account in the present numerical analysis examining the stability of HQV.

The results in Fig. 4 have been derived by choosing Eq. (21) as the initial configuration of the numerical run. The corresponding results of $|A^{(+)}_{-+}|$ and $|A^{(+)}_{--}|$, which describe the order parameter distribution accompanying the partner of the same HQV pair, are similar to those in Fig. 4. On the other hand, the corresponding results of a HQV of which the relative sense of the vorticity is *opposite* to that of the chirality are shown in Fig. 5 which are obtained by adopting Eq. (22) as the initial configuration of the numerical run. It is seen that the region with the reversed chirality close to the core is clearly narrower compared with that in Fig. 4.

Although the above-mentioned dependence of the core structure on the relative sense between the vorticity and the chirality was also seen in a previous GL analysis with no Fermi liquid (FL) correction included [24], the dependence of the vortex energy on this relative sense has not been examined
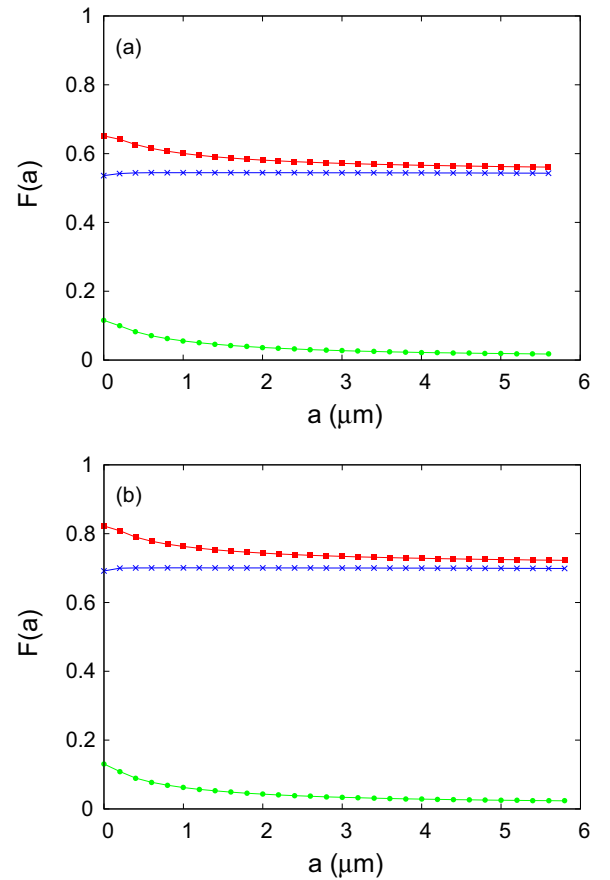

FIG. 6. Dependencies of the vortex energy of a HQV pair on the pair size $2a$. The red curve denotes the total energy $F(a)$ of one HQV pair, the blue curve is the contribution to $F(a)$ of the quadratic gradient term (24), and the green curve is the corresponding one of $O(|\Delta|^4)$ gradient energy $f_{FLgrad4}$ (see the text). (a) expresses the results in the case of Fig. 4, while (b) expresses those in the case of Fig. 5, respectively. The difference in $F(a)$ between the two cases is estimated to be about $0.25F(a)$ in the present study using the system size 40×8 (μm^2). The HQV pair studied in (a) and (b) has been created in terms of the same set of parameter values as in Figs. 4 and 5.

in the previous works [21,24,27]. Figure 6 expresses the dependencies on the HQV pair size $2a$ of the total energy $F(a)$ of a HQV pair, the corresponding quadratic gradient energy [Eq. (24)], and the $O(|\Delta|^4)$ gradient energy including the FL correction term. Figure 6(a) [6(b)] is the result in the case with the same (opposite) sense between the vorticity and the chirality. It is found that the HQV pair with the same relative vortex-chirality sense is lower in energy than that with the opposite relative sense. In both cases, the total energy (red curve) decreases slowly with increasing a, reflecting the a dependence of the $O(|\Delta|^4)$ gradient energy (green curve) [21] in each case. The difference in $F(a)$ between the two figures is found to arise from the corresponding difference in the quadratic gradient energy. Since, as already noted, both of the cases have the same energy in the London limit, it is clear that the origin of this difference is closely related to the order parameter component with the reversed orbital chirality appearing close to the core in Figs. 4 and 5. Reflecting
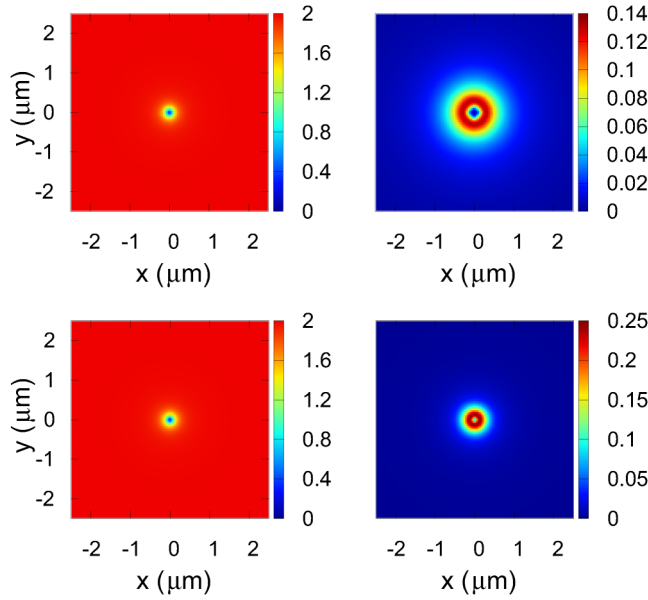
FIG. 7. Spatial distributions of the order parameter components of a PV realized in $a \to 0$ limit of Fig. 6 in the compatible (upper two figures) and the incompatible (lower two figures) configurations. The upper-left and upper-right figures express $A_{x+}^{(+)}$ and $A_{x-}^{(+)}$, respectively. The lower-left and lower-right figures express $A_{x-}^{(-)}$ and $A_{x+}^{(-)}$, respectively. We note that, in all figures, the vortex winding number is $+1$. The spin index x implies that the d- vector around this PV is spatially uniform and directed to the x axis (see the text).

this lift of the degeneracy on the relative sense between the vorticity and the chirality, hereafter the cases with the same and opposite senses between the vorticity and the chirality will be called *compatible* and *incompatible* configurations, respectively.

It is well understood that, in a p-wave Fermi superfluid with the order parameter field consisting of multicomponents, the vortex energy tends to be lowered by replacing the normal core of the conventional vortex with a superfluid core formed by a couple of components of the order parameter. Even in the present issue, a lower HQV energy is realized by inducing, close to the core, the order parameter component with the orbital chirality opposite to that of the order parameter far from the core. To explain how the vortex energy is lowered in the present system, for simplicity, we focus below on the core structure of the PV which is the $a \to 0$ limit of a HQV pair, because the order parameter structure close to the core of a PV is qualitatively similar to that of a HQV represented in the spin chiral basis [24]. In fact, as is seen in Fig. 7, the spatial distributions of the component with the reversed orbital chirality close to the PV core seem to be essentially the same as the corresponding ones of HQVs in Figs. 4 and 5. We note that, as a result of coalescence of the two HQVs with different spin chiralities from each other, the order parameter accompanying the resulting PV takes the form $A_{x,j}^{(\pm)}$, where j is an orbital index. That is, the d vector of the resulting PV is uniform and is directed to the x axis in our numerical results [see also Eq. (21)]. Consequently, the PV is described as well as a single HQV by *two* complex scalar components of the order parameter tensor $A_{\mu,j}$.
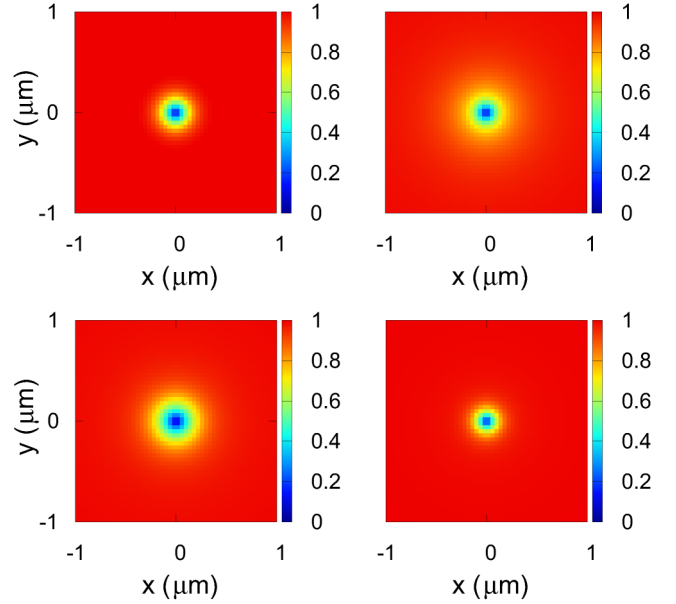

FIG. 8. Spatial distributions of the order parameter components defined in Eq. (32) accompanying a PV in the compatible (upper two figures) and the incompatible (lower two figures) configurations, respectively. The upper-left and upper-right figures express the results of $|A_{xr}^{(+)}|$ and $|A_{x\phi}^{(+)}|$, respectively, while the lower-left and lower-right figures express the results of $|A_{xr}^{(-)}|$ and $|A_{x\phi}^{(-)}|$, respectively.

To clarify the consequence of the component of the reversed orbital chirality induced close to the core, the p-wave superfluid order parameter $d_\mu^{(\pm)}(\hat{\mathbf{p}}) = A_{\mu,j}^{(\pm)} \hat{p}_j$ in the presence of a HQV pair in the compatible $(+)$ and incompatible $(-)$ configurations will be rewritten in the form

$$d_\mu^{(\pm)}(\hat{\mathbf{p}}) = A_{\mu,r}^{(\pm)} \hat{p}_r + A_{\mu,\phi}^{(\pm)} \hat{p}_\phi. \tag{31}$$

Here, $\hat{p}_r$ ($\hat{p}_\phi$) is the component of the unit vector $\hat{p}$ in the radial (azimuth) direction in the cylindrical coordinate system where the vortex center is at its origin, and

$$A_{\mu,r}^{(\pm)} = \tfrac{1}{2}(A_{\mu+}^{(\pm)} e^{i\phi} + A_{\mu-}^{(\pm)} e^{-i\phi}),$$
$$A_{\mu,\phi}^{(\pm)} = \tfrac{i}{2}(A_{\mu+}^{(\pm)} e^{i\phi} - A_{\mu-}^{(\pm)} e^{-i\phi}). \tag{32}$$

In Fig. 8, the spatial distributions of the order parameter components of the PVs in the compatible and incompatible configurations are shown based on the representation of Eq. (32). Regarding the ϕ dependencies in each case, $A_{x+}^{(+)}$ and $A_{x-}^{(+)}$ in the compatible case are approximately proportional to $e^{i\phi}$ and $e^{i3\phi}$, respectively, and the resulting quantities $A_{x+}^{(+)} e^{-i\phi}$ and $A_{x-}^{(+)} e^{-i3\phi}$, which are functions of the radius r, are real and have the same sign as each other. On the other hand, the corresponding quantities $A_{x+}^{(-)}$ and $A_{x-}^{(-)}$ in the incompatible case are approximately proportional to $e^{-i\phi}$ and $e^{i\phi}$, respectively, and the quantities $A_{x+}^{(-)} e^{i\phi}$ and $A_{x-}^{(-)} e^{-i\phi}$ are real and have the opposite sign to each other. These results are consistent with the features seen in the previous work [24]. It is found that, in the compatible case, the superfluid core is maintained over a wider range in the radial direction, while in the incompatible case, the nonvanishing order parameter amplitude is remarkably seen rather in the azimuth direction, and consequently,

the normal region in the core seems to be wider in the radial direction. These features imply that the superfluid weight in the core region is wider in the compatible configuration and well explains the result seen in Fig. 6 that the vortex energy is lower in this case. It will be clear that, according to Fig. 6, this explanation on the lift of the degeneracy due to the relative sense between the vorticity and the chirality also holds for a HQV pair with a nonvanishing size $2a$. In the remainder of this section, for simplicity, we will not distinguish a PV from a HQV pair, and they will be called just a "vortex."

In considering possible vortex states in the chiral phase in a planar aerogel under a rotation, we need to take account of randomness on the surface of the defect planes. In general, some randomness in the x-y plane will create the chiral domains. Namely, the **l** vector oriented perpendicularly to the x-y plane may be directed to the $+\hat{z}$ or $-\hat{z}$ directions on each defect plane depending on the smoothness of the surface of each defect, and the randomness-induced domain walls separating the $\hat{l} \parallel -\hat{z}$ region from the $\hat{l} \parallel \hat{z}$ region are present.

Once taking account of both the presence of the chiral domains and the energy difference between the vortices in the compatible and incompatible cases, nontrivial vortex states are expected to occur in the chiral superfluid phase in a planar aerogel. First, the dependence of a single vortex energy on the relative sense between the vorticity and the chirality implies that the broken time-reversal symmetry of the chiral A phase is reflected in the vortex lattice structure. That is, a vortex lattice created on a random configuration of the chirality, as sketched in Figs. 9(a) and 9(b), does not coincide with the corresponding vortex state occurring after the rotation direction is reversed. In the Fig. 9(a), the rotation-induced vortices are compatible, over a large area in the x-y plane, with the chirality $\hat{l} \parallel \hat{z}$, which is indicated by the two arrows orthogonal to each other, while the rotation-induced vortex inside the ellipse (solid curve) expressing a domain wall has a higher energy and hence, may not appear in equilibrium. By contrast, in the Fig. 9(b), the rotation-induced vortices are incompatible over a large area with the chirality $\hat{l} \parallel -\hat{z}$, and thus, the vortices prefer to stay inside the same chiral domain as that included in Fig. 9(a). Therefore, the presence of more chiral domains would lead to a larger difference in the vortex lattice structure when the rotation direction is reversed.

Further, the vortex energy dependent on the relative sense also suggests the presence of a vortex-antivortex pair or a vortex loop supported by the pinning to the planar defects. For instance, as sketched in Fig. 9(c), the rotation-induced vortex is favored in the elliptic domain in Fig. 9(b), while the "antivortex" with the opposite sense to the rotation has a lower energy outside it. Then, a vortex loop may appear depending on the situation due to the presence of the chiral domains. We stress that the presence of the planar defects forming the planar aerogel assists the appearance of such a vortex loop: In general, the extended or correlated defects strongly pin the vortex segments. In fact, all the vortices appearing in the nematic aerogels are extended along the linelike strands because of the pinning due to them [20]. Similarly to this, a vortex segment extended along the planar defects tends to be stabilized, as in Fig. 9(d), because of the pinning effect due to the planar defects. Therefore, such vortex loops may
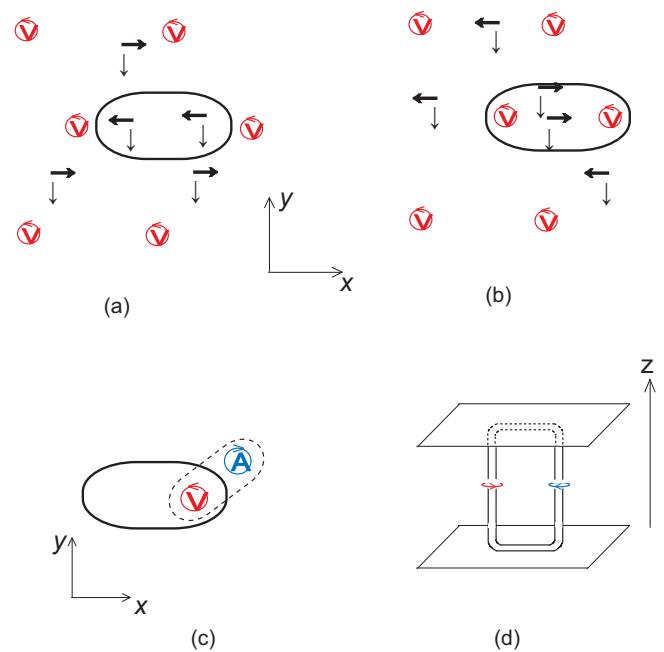

FIG. 9. (a) Schematic figure of a possible defective vortex lattice created by a rotation angular velocity $\Omega > 0$ in the globally compatible situation (i.e., with $\hat{l} \parallel \hat{z}$ over a large area). A symbol V denotes a rotation-induced vortex. A chiral domain wall is indicated by an ellipse. Hence, we have the incompatible situation inside the chiral domain, and thus, it was assumed that no rotation-induced vortices are present there. (b) Corresponding figure in the globally incompatible situation (i.e., with $\hat{l} \parallel -\hat{z}$ over a large area). In this case, the rotation-induced vortices prefer to stay in the chiral domain where $\hat{l} \parallel \hat{z}$. (c) Possible configuration of one vortex pair (or, vortex loop) to be realized in the situation of (b). In this case, both a rotation-induced vortex inside the chiral domain and an antivortex (denoted as the symbol A) outside it are compatible with the chirality. (d) The 3D picture drawing the vortex-antivortex pair indicated in (c) as a vortex loop. Here, the upper and lower planes denote planar defects composing the aerogel locally. The segments of the vortex loop perpendicular to the z axis will be strongly pinned by the defect planes so that such a vortex loop does not easily disappear.

be realized in equilibrium with no substantial energy cost as the chiral domains increase.

IV. SUMMARY AND DISCUSSION

Motivated by the recent experiment [8] on superfluid ³He in the planar aerogels composed of randomly stacked planar defects, we have extended the impurity scattering model used in the previous study [2] on the superfluid phase diagram in the uniaxially compressed aerogel to the case in which the quasiparticle scattering on the planar defects is close to the specular limit. This specular limit corresponds to the limit of strong planar anisotropy and to one situation in which an analog of the Anderson's theorem for the s-wave paired superfluid is satisfied for a p-wave Fermi superfluid. In this limit, the only superfluid phase to be realized in such an aerogel is the chiral A phase in which its $\hat{l}$ vector is kept perpendicular to the defect planes. We have examined the resulting phase

diagram in the case of a moderately strong anisotropy and have explained the main features seen experimentally [8], such as the superfluid transition temperature quite close to that of the bulk liquid and the chiral A phase stabilized over wide pressure and temperature ranges. Further, we have argued that the T^4 behavior of the quasiparticle energy gap to be seen in the bulk A phase if this phase is realized at low temperatures may not be necessarily satisfied in the chiral A phase in a planar aerogel, although the point node of the energy gap is robust against the impurity scattering effect.

We have also studied stable vortices in the chiral A phase in planar aerogels. It is well known that the core of a single HQV realized in the A phase with a fixed direction of the chirality is one of the ideal systems for realizing Majorana modes [28,29],

and the stability of a HQV in the present system is also a subject of much interest. First, we have pointed out that, for both the half-quantum vortex and the conventional phase vortex, the vortex energy depends on the relative sense between the vorticity and the orbital chirality. By combining this feature with the fact that the chiral domains tend to be realized due to the randomness on the defect planes, we have argued a possible reflection of the broken time-reversal symmetry in the vortex lattice structure and the appearance of the vortex loops stabilized by the pinning of the transverse vortex segments due to the defect planes. Observing a dependence of the vortex lattice structure on the rotated direction would become evidence of the presence of the chirality [30,31] in the high temperature equal-spin paired state in the planar aerogels.

[1] V. V. Dmitriev, A. A. Senin, A. A. Soldatov, and A. N. Yudin, Phys. Rev. Lett. **115**, 165304 (2015).

[2] K. Aoyama and R. Ikeda, Phys. Rev. B **73**, 060504(R) (2006).

[3] I. A. Fomin, J. Exp. Theor. Phys. **127**, 933 (2018).

[4] T. Hisamitsu, M. Tange, and R. Ikeda, Phys. Rev. B **101**, 100502(R) (2020).

[5] W. F. Brinkman, J. W. Serene, and P. W. Anderson, Phys. Rev. A **10**, 2386 (1974).

[6] J. A. Sauls and J. W. Serene, Phys. Rev. B **24**, 183 (1981).

[7] J. Pollanen, J. I. A. Li, C. A. Collett, W. J. Gannon, W. P. Halperin, and J. A. Sauls, Nat. Phys. **8**, 317 (2012).

[8] V. V. Dmitriev, M. S. Kutuzov, A. Y. Mikheev, V. N. Morozov, A. A. Soldatov, and A. N. Yudin, Phys. Rev. B **102**, 144507 (2020).

[9] P. W. Anderson, J. Phys. Chem. Solids **11**, 26 (1959).

[10] V. B. Eltsov, T. Kamppinen, J. Rysti, and G. E. Volovik, arXiv:1908.01645.

[11] A. B. Vorontsov and J. A. Sauls, Phys. Rev. Lett. **98**, 045301 (2007).

[12] Y-H. Li and T-L. Ho, Phys. Rev. B **38**, 2362 (1988).

[13] D. Volhardt and P. Wolfle, *The Superfluid Phases of Helium 3* (Taylor & Fransis, London, 2003).

[14] V. Ambegaokar, P. G. de Gennes, and D. Rainer, Phys. Rev. A **9**, 2676 (1974).

[15] A. A. Abrikosov, L. P. Gor'kov, and I. E. Dzyaloshinski, *Methods of Quantum Field Theory in Statistical Physics* (Dover, New York, 1963), Sec. 39.3.

[16] R. Balian and N. R. Werthamer, Phys. Rev. **131**, 1553 (1963).

[17] In the 3D superfluid ^{3}He in a globally isotropic aerogel, the impurity-induced reduction of $T_c(P)$ can be partly suppressed by taking account of the spatial inhomogeneity of the order parameter. See R. Hanninen and E. V. Thuneberg, Phys. Rev. B **67**, 214507 (2003).

[18] T. W. B. Kibble, J. Phys. A **9**, 1387 (1976).

[19] W. H. Zurek, Nature (London) **317**, 505 (1985).

[20] J. T. Makinen, V. V. Dmitriev, J. Nissinen, J. Rysti, G. E. Volovik, A. N. Yudin, K. Zhang, and V. B. Eltsov, Nat. Commun. **10**, 237 (2019).

[21] N. Nagamura and R. Ikeda, Phys. Rev. B **98**, 094524 (2018).

[22] T. Hisamitsu and R. Ikeda, arXiv:2103.12460.

[23] M. M. Salomaa and G. E. Volovik, Phys. Rev. Lett. **55**, 1184 (1985).

[24] K. Kondo, T. Ohmi, M. Nakahara, T. Kawakami, Y. Tsutsumi, and K. Machida, J. Phys. Soc. Jpn. **81**, 104603 (2012).

[25] N. Hayashi and Y. Kato, J. Low Temp. Phys. **131**, 893 (2003).

[26] M. Tange and R. Ikeda, Phys. Rev. B **101**, 094512 (2020).

[27] T. Ohmi, M. Nakahara, T. Tsuneto, and T. Fujita, Prog. Theor. Phys. **68**, 1433 (1982).

[28] N. Read and D. Green, Phys. Rev. B **61**, 10267 (2000).

[29] D. A. Ivanov, Phys. Rev. Lett. **86**, 268 (2001).

[30] H. Ikegami, Y. Tsutsumi, and K. Kono, Science **341**, 59 (2013).

[31] J. Kasai, Y. Okamoto, K. Nishioka, T. Takagi, and Y. Sasaki, Phys. Rev. Lett. **120**, 205301 (2018).